SASEC2015
Third Southern African Solar Energy Conference
11 – 13 May 2015
Kruger National Park, South Africa

EFFECT OF DOPING ON ZnO BASED TRANSPARENT CONDUCTING OXIDES AND DOWN/UP CONVERSION PHOSPHOR FOR SOLAR CELL APPLICATION

Vinod Kumar[1,*], H.C. Swart[1,*], Vijay Kumar[1], Anurag Pandey[1], L.P. Purohit[2] and O.M. Ntwaeaborwa[1]

[1]Department of Physics, University of the Free State, Bloemfontein, ZA9300, South Africa

[2]Department of Physics, Gurukula Kangri University, Haridwar 249 404, India

E-mail: vinod.phy@gmail.com
swarthc@ufs.ac.za

ABSTRACT

Boron doped ZnO (ZnO:B) films were grown by the spin coating method. The structure of the ZnO:B film has been found to exhibit the hexagonal wurtzite structure. A minimum resistivity was obtained to be 7.9×10^{-4} Ω-cm at 0.6 at.% of B concentration in the ZnO:B films. The optical interference pattern in the transmittance spectra shows good homogeneity with a transparency of ~91%, in the visible region. The efficiencies of the dye sensitized solar cell (DSSCs) formed using the ZnO:B window layers were obtained to be 1.56 %. Rare earth doped oxide based nano-phosphors for up and down conversion applications were also synthesised by a solution combustion method. The efficiency of the DSSC can be enhanced by using an extra layer of down and up conversion phosphor material as a layer on top of the solar cell.

INTRODUCTION

Transparent conducting window layer materials such as Zinc oxide (ZnO), Indium tin oxide (ITO) and fluorine doped tin oxide (FTO) play a very important role in solar cell technologies such as dye sensitized solar cell (DSSCs), quantum dot sensitized solar cells (QDSSCs), polymer solar cells and hybrid solar cells [1-4]. The advantages of DSSCs are its low fabrication cost, flexibility and efficiency [1-4]. Usually, TiO_2 films are used as the transparent conducting oxide (TCO) in DSSCs because of their adequate surface area and chemical affinity for the dye adsorption as well as their suitable energy band potential alignment for charge transfer. However, the numerous grain boundaries between the TiO_2 nano-particles (NPs) restrict fast electron transport, which is detrimental to the efficient energy conversion process [5, 6]. Recently, ZnO NPs have been explored as alternatives to TiO_2 as an electron conductor. Bulk ZnO has a unique combination of electrical and optical properties, including relatively high electron mobility (more than 1 order of magnitude larger than anatase TiO_2) [5, 6]. In addition, ZnO has a rich family of nanostructures with diverse applications in optoelectronics and photovoltaics [7-10]. This unique combination of properties has opened possibilities for using ZnO to improve the performance of photovoltaic cells. For example, ZnO showed the first experimental evidence of irreversible electron injection from organic molecules into the conduction band of a wide band gap semiconductor [11]. Nowadays, ZnO is emerging as an efficient electron transport material in technologies such as DSSCs and inverted polymer solar cells, QDSSCs, bio-medical applications and light emitting diodes [12-16].

Up-conversion (UC) and down-conversion (DC) of sunlight are two possible routes for improving energy harvesting over the whole solar spectrum. Via such processes it could be possible to exceed the Shockley-Queisser limit for a single-junction photovoltaic (PV) device [17]. The effect of adding DC and UC layers to the front and rear of a solar cell, respectively, is to modify the incident solar spectrum. One of the materials more extensively studied for these propose have been the lanthanides or rare-earth systems, due to the suitability of their discrete energy levels for photon conversion inside a wide variety of host materials. While high quantum yields of 200% have been demonstrated with DC materials, there remain several barriers to realising such a layer that is applicable to a solar cell. These are, firstly, weak absorption of the lanthanide ions and, secondly, the competing loss mechanism of non-radiative recombination. For UC, these two barriers still exist, however an additional challenge is the non-linear nature of the UC process, thus favouring operation under concentrated sunlight. In this paper, we review the application of UC and DC to the solar cell, discussing the material systems used and optical characterisation [18].

In the paper, the effect of Boron (B) doping concentration on the electrical and optical properties of ZnO:B is investigated. The optimized thin film is used as a window layer in DSSC. The PL of possible UP and DC materials are also investigated.

EXPERIMENTAL DETAIL

Boron doped ZnO (ZnO:B) thin films have been deposited on a microscopic corning glass substrate using the

spin coating technique. Zinc acetate dihydrate (Alfa Aesar) was used as a starting material. Methanol (AR, Merck) and monoethanolamine (MEA, Merck) were used as solvent and stabilizer, respectively. The zinc precursor solution was prepared by dissolving zinc acetate dihydrate in methanol so as to prepare concentration of 0.2 mol/l. Then MEA was dissolved into the solution. The molar ratio MEA/Zn was fixed to 1 for all samples. Trimethyl borate was also dissolved into the solution to obtain ZnO:B solution. Boron concentration was varied from 0 to 1 at.%. The mixed solution was stirred by using a magnetic stirrer at 25ºC for 2 h. The transparent and homogenous solution was obtained after 72 h. The solution was dropped onto the glass substrate, which was rotated at 2500 r/min for 30 s by a spin coater. After deposition, the films were dried in air at 230ºC for 10 min over a hot plate to evaporate the solvent and remove organic residuals. The procedures for coating to drying were repeated 15 times until the desired thickness. The films were then inserted to a microprocessor controlled furnace for annealing in air at 450ºC for 1 h.

Films of ZnO NPs (thickness ~10 µm) were deposited on ZnO:B thin films using the doctor blade technique [19]. N3 dye was used as a sensitizer. The deposited ZnO film was immersed in a 0.3 mM solution of N3 dye in ethanol for 24 h. The dye covered electrodes were then rinsed with ethanol to remove the excess dye from surface and dried at room temperature. The dye coated assembly was then dipped into gel electrolyte for 1 h. The gel electrolyte was prepared by using a 10% polyethylene oxide (PEO 99%, Alfa Aesar) solution in acetonitrile and carbon nanotubes (CNTs, 90 + %, Alfa Aesar) with LiI 0.1 M (9.95%, Alfa Aesar), and I_2 0.015 M (99.8 %, Alfa Aesar). The whole mixture was placed for sonication to disperse the CNTs into the polymer matrix. The mixture was stirred for 10 h with a magnetic stirrer in order to get a complete mixing between the CNTs and the polymer molecules. A thin platinum sheet was used as counter electrode.

ZnO:Ce^{3+}, ZnO:Tb^{3+} and Er^{3+}-Yb^{3+} co-doped $SrWO_4$ NPr were also synthesised for possible UC and DC materials by using the solution combustion method. The source material and urea were mixed and dissolved in distilled water. Dopant nitrate was used as the dopant source in the solution. A homogeneous solution was obtained after stirring for 20 min. The solution was transferred to a pre-heated muffle furnace maintained at a temperature of 450±10°C. All the liquid evaporated and a large amount of heat was released which resulted into a flame that decomposed the reagents further and released more gases. The flame lasted for 60 s and the combustion process was completed within 5 min. The resulting DC and UP powders were cooled down to room temperature and ground gently using a pestle and mortar.

RESULTS AND DESSCUSION

X-ray diffraction (XRD) patterns of ZnO:B films prepared by sol-gel process are shown in Figure 1. It indicates that most of the grains in ZnO:B have a strong orientation along the *c*-axis (002) plane as reported in JCPDS card No. 79-0206. The intensity of the (002) peak has increased with increasing B concentration up to 0.6 at.% and then the intensity of the (002) peak has decreased. This behaviour can be understood by two competing processes; the increase of boron doping improves the stoichiometry of the films and the crystal quality. This indicates that boron ions are substituted at zinc ions sites up to 0.6 at.% after that B-B intra grain cluster is evaluated.

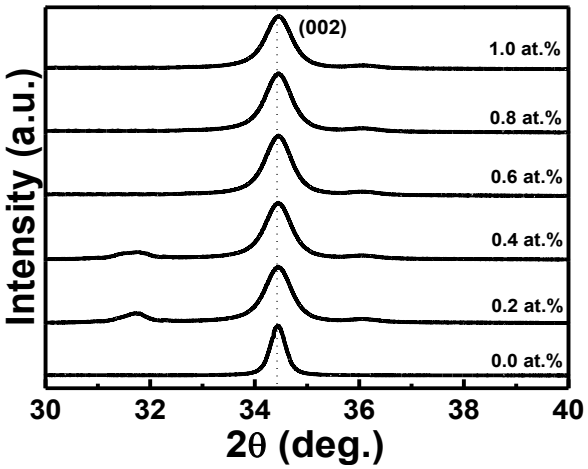

Figure 1 XRD pattern of ZnO:B films as a function of boron concentration

Figure 2 depicts the variation of electrical resistivity and carrier concentration in ZnO:B thin films as a function of B concentration. The electrical resistivity of ZnO:B film has decreased with increasing B concentration. A minimum resistivity was obtained to be 7.9×10^{-4} Ω-cm at 0.6 at.% of B. The resistivity of ZnO:B films has decreased due to contribution of extra free electrons of B^{3+} ions substituting into the Zn^{2+} ions sites. The resistivity was found to increase at higher doping concentration of boron (0.8 and 1.0 at.%) because excess B might result in intra grain forming B-B cluster. Similar suggestions about intra grain cluster were proposed by Lu et al.[20] and Yu et al.[21] for ZnO:Al and ZnO:Y films, respectively. The carrier concentration has increased with increasing B concentration up to 0.6 at.% and the largest value of carrier concentration 6.26×10^{20} cm^{-3} at 0.6 at.% B was obtained. Then the carrier concentration has decreased with a further increase in B concentration due to intra grain cluster scattering [22].

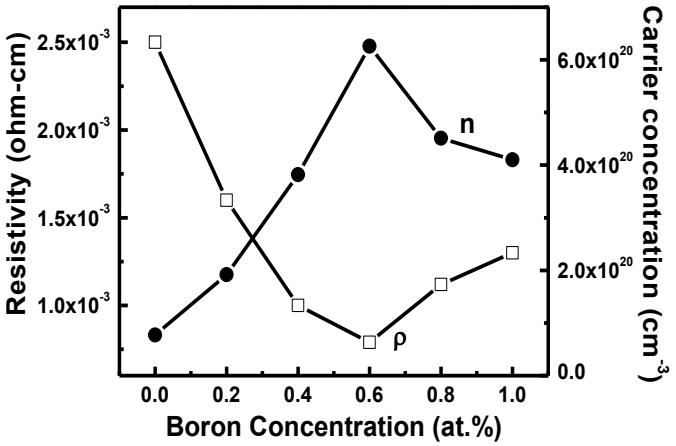

Figure 2 Effect of boron doping on the resistivity and carrier concentration of ZnO:B films,

Figure 3 shows the optical transmittance spectra in the wavelength range of 300 to 800 nm of the ZnO:B thin films at different doping concentration. Optical interference in the transmittance spectra shows a homogenous nature of the films. The transmittance of the film has increased with increasing doping concentration and a maximum transmittance was obtained of 88% at 0.6 at.% of B. The increase in the transmittance at 0.6 at.% of B may be due to decreasing optical scattering caused by the densification of grains followed by grain growth and the reduction of grain boundary density as demonstrated. Since we are mainly interested in measuring the optical band gap of films, many criteria have been used to define the onset of inter band transitions in direct band gap semiconductors. The transition energy could be simply deduced from the zero crossing of the second derivative of the absorption spectrum. The Fermi exclusion principle, optical transitions can only occur for higher photon energies to make vertical transitions from the valence band up to the state with Fermi momentum in the conduction band. A blue shift in ultraviolet (UV) absorption edge is observed with increasing concentration, indicating the broadening of the optical band gap.

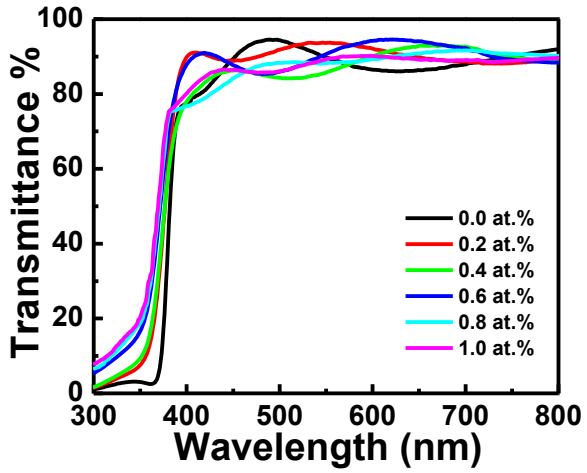

Figure 3 Optical transmittance spectra of ZnO:B films for different boron concentration

The optical band gap was calculated by using Tauc's plot method [22]

$$\alpha h\nu = B\left(h\nu - E_g\right)^{1/2} \quad (9)$$

Where, α is the absorption coefficient, h is the plank's constant and ν is frequency of incident photon, E_g is the optical band gap and B is a constant, α is evaluated using

$$\alpha = \frac{1}{d}\ln\left(\frac{1}{T}\right) \quad (10)$$

Where, T is the transmittance of the film and d is the thickness of film. The plot of $(\alpha h\nu)^2$ versus $h\nu$ for ZnO:B at different concentration of B is shown in Figure 4. The optical band gap (Eg) was obtained by extrapolating the linear part of the Tauc's plot to intercept the energy axis at $(\alpha h\nu)^2 = 0$. The band gap of the films was found to increase continuously from 3.24 to 3.35 eV with an increase in the concentration. The change in the optical band gap was analyzed in terms of Burstein- Moss (B-M) band gap widening [22].

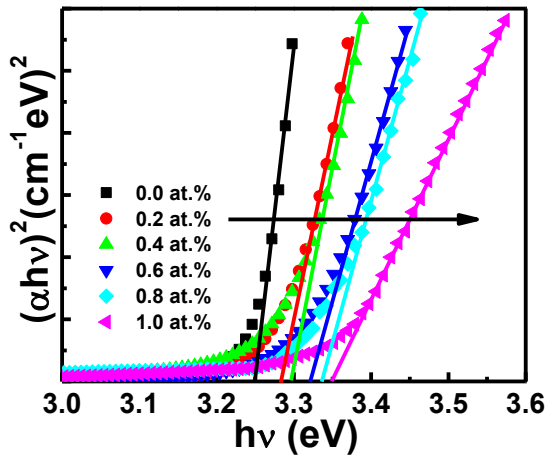

Figure 4 band gap variation of ZnO:B films with boron concentration

I-V MEAURMENT OF SOALR CELL

As pointed out above, the sandwich type DSSCs were fabricated using the ZnO:B window layer films as front electrodes (topmost layer in schematic diagram). The synthesized ZnO NPs was used as host material (bigger spheres), the N3 dye as active layer (smaller spheres), I^-/I_3^- electrolyte for charge separation and Pt as counter electrode (bottom layer). The cell was illuminated under one sun illumination (AM 1.5, 100 mW/cm^2) and I-V characteristics of the cells were obtained using a Keithley source meter. I-V curves of the DSSCs with different window layers are shown in Figure 5. The efficiency of the ZnO:B based DSSC was obtained as 1.56%.

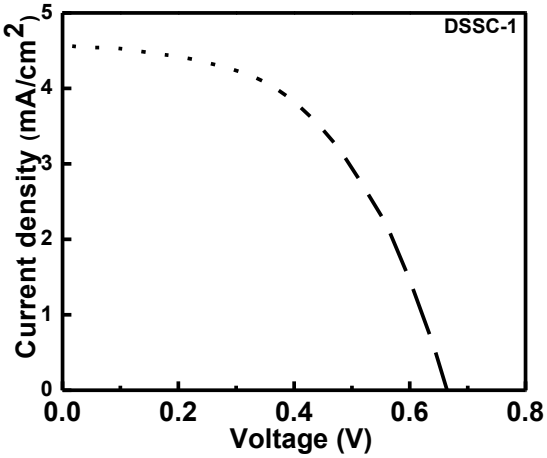

Figure 5 I-V characteristic of ZnO:B window layer based DSSC

DOWN CONVERSION MATERIAL

ZnO:Tb^{3+} and ZnO:Ce^{3+} materials were synthesized for possible DC material. The PL emission curve of the ZnO:Tb^{3+} material excited by 325 is shown in Figure 6. For the ZnO:Tb^{3+}, a major green emission peak at 543 nm and a few minor peaks at 489, 586, 622, 444 and 420 nm were detected. These peaks represent the $^5D_4$-$^7F_5$, $^5D_4$-$^7F_6$, $^5D_4$-$^7F_4$, $^5D_4$-$^7F_3$, $^5D_3$-$^7F_4$ and $^5D_3$-$^7F_5$ transitions of Tb^{3+}, respectively [23, 24].

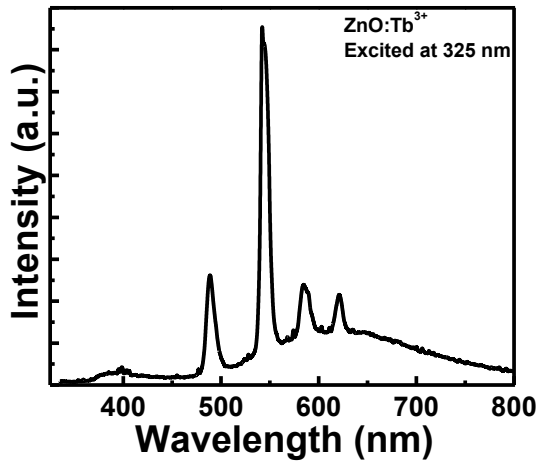

Figure 6 PL emission curve of ZnO:Tb^{3+} NPr excited by 325 nm laser.

The PL emission curve of ZnO:Ce^{3+} material excited by 248.6 nm line of a Ne Cu laser is shown in Figure 7. According to the reported values in literature [25], the transitions in a Ce^{3+} doped ZnO lattice may be attributed to (i) 399-404nm exciton emission (ii) 417nm ($^5D_0$–4F) (characteristic emission of Ce^{3+}) (iii)426-428 nm ($^5D_4$–$^4F_1$) (iv) 448-452 nm ($^5D_0$–$^7F_1$) (v) 468 nm ($^5D_2$–$^7F_0$) (vi) 553-566 nm ($^5D_4$–F_j) (vii) 601nm ($^5D_0$-$^7F_1$) (viii) 629 nm ($^5D_0$–$^7F_2$). Although not very efficient in the case of the Ce doped ZnO both materials maybe used as possible DC materials.

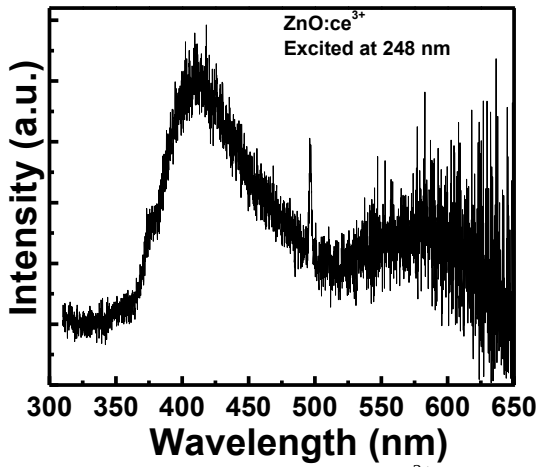

Figure 7 PL emission curve of ZnO:Ce^{3+} NPr excited by 248 nm laser.

UP CONVERSION MATERIAL

The UC emission spectra of the Er^{3+}-Yb^{3+} co-doped $SrWO_4$ phosphor recorded in the 400-900 nm range upon a 980 nm excitation is shown in figure 8. Two dominant green UC emission bands have been marked along with the comparatively weak blue, red and NIR bands. These emission bands are peaking at about 409, 525, 547, 658 and 800 nm and assigned for the $^2H_{9/2}\rightarrow{}^4I_{15/2}$, $^2H_{11/2}\rightarrow{}^4I_{15/2}$, $^4S_{3/2}\rightarrow{}^4I_{15/2}$, $^4F_{9/2}\rightarrow{}^4I_{15/2}$ and $^4I_{9/2}\rightarrow{}^4I_{15/2}$ transitions of the Er^{3+} ion and about 489 nm due to the $^2F_{5/2}\rightarrow{}^2F_{7/2}$ transition of the Yb^{3+}ion, respectively [26, 27]. It may therefore be used as a UC material.

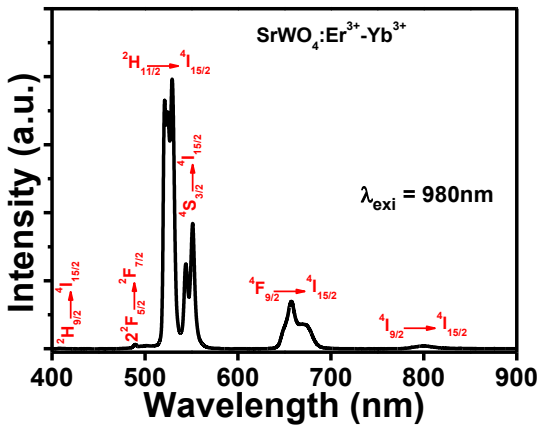

Figure 8 PL emission curve of $SrWO_4$:Ce^{3+}-Yb^{3+} NPr excited by 980 nm laser.

CONCLUSION

DSSCs were fabricated using highly transparent and conducting ZnO:B thin films as front window electrodes with crystalline ZnO NPs as host material. The efficiencies of the DSSCs fabricated using the ZnO:B as window layers were obtained to be 1.56 %. These results demonstrate that these highly transparent and conducting ZnO:B thin films are promising candidates for window layer application in DSSC. The UC and DC materials for enchantment of the efficiency of DSSC were successfully synthesized.

ACKNOWLEDGEMENT

This work is based on the research supported by the South African Research Chairs Initiative of the Department of Science and Technology, and the National Research Foundation of South Africa. The PL system used in this study is supported both technically and financially by the rental pool programme of the National Laser Centre. The financial support from the University of the Free State is highly recognized. Authors are grateful to Prof. J.R. Botha, Nelson Mandela Metropolitan University, Port Elizabeth, South Africa for providing the PL measurement facility.

REFERENCES

[1] B. Oregan and M. Gratzel, Nature, **353,** 737 (1991).
[2] H. Liu, V. Avrutin, N. Izyumskaya, U. Ozgur and H. Morkoc, Superlattices Microstruct, **48**, 458 (2010).
[3] D. Dimova-Malinovska, **253,** 012007-15 (2010)

[4] C. Y. Jiang, X. W. Sun, K. W. Tan, G. Q. Lo, A. K. Kyaw, and D. L. Kwong, Appl. Phys. Lett., **92**, 143101 (2008).
[5] D. C. Look, D. C. Reynolds, J. R. Sizelove, R. L. Jones, C. W. Litton, G. Cantwell, and W.C. Harsch, Solid State Commun., **105**, 399 (1998).
[6] L. Forro, O. Chauvet, D. Emin, L. Zuppiroli, H. Berger, and F. Levy, J. Appl. Phys., **75**, 633 (1994).
[7] X. Jin, M. Gotz, S. Wille, Y. K. Mishra, R. Adelung and C. Zollfrank, Adv. Mater., **25**, 1342 (2013).
[8] C. Klingshirn, Chem. Phys. Chem. **8**, 782 (2007).
[9] V.-M. Guerin and T. Pauport, Energy Environ. Sci. **4,** 2971 (2011).
[10]Y. K. Mishra, S. Mohapatra, R. Singhal, D. K. Avasthi, D. C. Agarwal and S. B. Ogale, Appl. Phys. Lett. **92**, 043107 (2008).
[11] H. Tributsch and M. Calvin, Photochem. Photobiol. **14,** 95 (1971).
[13] J. Ajuria, I. Etxebarria, W. Cambarau, U. Muñecas, R. Tena Zaera, J. C. Jimeno, and R. Pacios, Energy Environ. Sci. **4**, 453 (2010).
[14] I. J. Kramer and E. H. Sargent, ACS Nano **5**, 8506 (2011).
[15] Y. K. Mishra, R. Adelung, C. Rohl, D. Shukla, F. Spors, and V. Tiwari, Antivir. Res. **92**, 305 (2011).
[16] O. Lupan, T. Pauporte and B. Viana, Adv. Mater. **22**, 3298 (2010).
[17] W.G. Sark, J. Wild, J.K. Rath, A. Meijerink and R. E. Schropp, Upconversion in solar cells, Nanoscale Research Letters **8,** 81 (2013).
[18] Y.-C. Chen, W.-Y. Huang, T.-M. Chen, Enhancing the performance of photovoltaic cells by using down-converting $KCaGd(PO4)_2:Eu^{3+}$ phosphors, J. of Rare earths, **29**(9), 907(2011).
[19] P. Suri and R. M. Mehra, Sol. Energy Mater. Sol. Cells, **91**, 518 (2007).
[20] J.G. Lu, Z.Z. Ye, Y.J. Zeng, L.P. Zhu, L. Wang, J.Yuan, B.H. Zhao and Q.L. Liang: J. Appl. Phys., **100**, 073714 (2006).
[21] Q. Yu, W. Fu, C. Yu, H. Yang, R. Wei, Y. Sui, S. Liu, Z. Liu, M. Li, G. Wang, C. Shao, Y. Liu and G. Zou: J. Phys. D: Appl. Phys., **40**, 5592 (2007), .
[22] Vinod Kumar, R.G. Singh, L.P. Purohit and R.M. Mehra, J. Mater. Sci. Technol., **27(6),** 481 (2011).
[23] Vinod Kumar, S. Som, V. Kumar, V. Kumar, O.M. Ntwaeaborwa, E. Coetsee, H.C. Swart, Chemical Engineering Journal, **255,** 541 (2014).
[24] A.S. Pereira, M. Peres, M.J. Soares, E. Alves, A. Neves, T. Monteiro, T. Trindade, Synthesis, surface modification and optical properties of Tb^{3+} doped ZnO nanocrystals, Nanotechnology, **17**, 834 (2006).
[25] N.R. Panda, B.S. Aecharya, T.B. Singh, R.K. Gartia, J. Lumin., **136**, 369 (2013).
[26] D. K. Mohanty, V. K. Rai, Y. Dwivedi, S. B. Rai, Appl. Phys. B, **104**, 233 (2011) .
[27] B. P. Singh, A. K. Parchur, R. K. Singh, A. A. Ansari, P. Singh, S. B. Rai, Phys. Chem. Chem. Phys., **15**, 3480(2013) .